molecules

MDPI

Article

Covalently Interconnected Conjugated Polymer–Polymer Heterojunctions: A Practical Approach for Photocatalyst Fabrication

Zheng-Tao Bao [1,2,†], Yu-Jie Zhang [1,2,†], Pachaiyappan Murugan [3,†], Kun-Ming Liu [1,*], Li-Qing Li [1,*], Fang Yang [2] and Shi-Yong Liu [1,2,*]

[1] School of Chemistry and Chemical Engineering, Jiangxi University of Science and Technology, Ganzhou 341000, China
[2] School of Chemical Engineering, Guangdong University of Petrochemical Technology, Maoming 525000, China
[3] Center for Global Health Research, Saveetha Medical College and Hospital, Saveetha Institute of Medical and Technical Sciences, Kancheepuram District, Chennai 602105, Tamil Nadu, India
* Correspondence: liukunmingjxust@126.com (K.-M.L.); liliqing79@126.com (L.-Q.L.); chelsy@gdupt.edu.cn or chelsy@zju.edu.cn (S.-Y.L.)
† These authors contributed equally to this work.

Abstract

Photocatalytic hydrogen gas generation through the utilization of π-conjugated polymers has gained popularity due to its diverse functional features and the simplicity with which it can be designed structurally. However, the rates of H_2 generation that these polymers generate are restricted due to the quick recombination of photoexcited electrons and holes. In order to facilitate charge-carrier separation and improve photocatalytic H_2 production, we have created chemically linked heterostructures of linear conjugated polymers. Using a method known as progressive polymerization, the benzenoid unit was selectively improved by the addition of dibenzothiophene-S, S-dioxide, and ethylene dioxythiophene, all of which perform electron-donating and electron-withdrawing activities, respectively. Photophysical and electrochemical analysis, which was corroborated by the hybrids' photophysical properties, indicated that the hybrids that were developed had a considerably enhanced charge-carrier separation efficiency for the hybrids. In contrast to the non-photocatalytic nature of the pure TPA-Ph polymer, the TPA-Ph@PPD-BSO_2 heterostructures show an optimal HER of up to 16.5 mmol g^{-1} h^{-1} when exposed to visible light ($\lambda > 420$ nm) without the presence of a Pt co-catalyst. This value is 1.5 times higher than that of single-component PPD-BSO_2. This study provides a practical synthetic protocol for fabricating covalently coupled polymer–polymer heterojunctions with enhanced interfacial charge dynamics for solar-to-chemical conversion.

Keywords: π-conjugated polymers; chemically linked heterostructures; photocatalysis; charge-carrier separation; Pt-free photocatalysis; direct arylation

Check for updates

Academic Editor: Ying-Wei Yang

Received: 21 October 2026
Revised: 20 November 2026
Accepted: 21 November 2026
Published: 25 November 2026

Copyright: © 2026 by the authors. Licensee MDPI, Basel, Switzerland. This article is an open access article distributed under the terms and conditions of the Creative Commons Attribution (CC BY) license.

1. Introduction

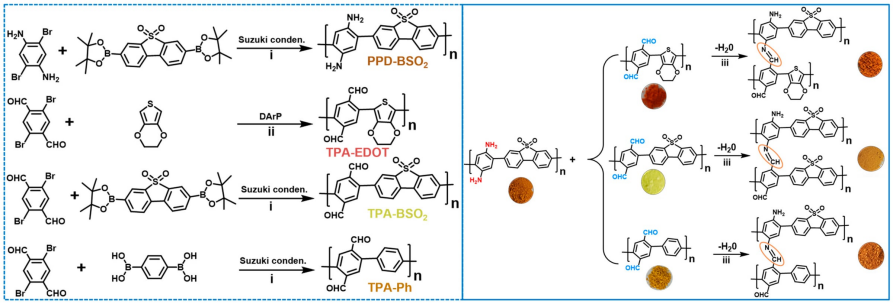
One of the most intriguing potential answers to future energy and environmental problems has been the use of photo-catalysts, which directly convert solar energy into hydrogen energy [1]. A lot of people think that hydrogen will be able to take the place of fossil fuels soon, and that our societies will be able to keep growing without endangering the environment [2–11]. Potential candidates have been identified as conjugated organic polymers (COPs) with advantageous features such as high stability, a large π-conjugated

system, adjustable properties, and flexible structures, ever since the pioneer polymer photocatalyst poly(p-phenylene) showed hydrogen evolution performance in 1990 [12–19]. There is still a significant gap in the as-prepared COPs' PHE performance, despite the enormous challenge of creating novel organic linear copolymers with high activity and low cost and pinpointing their exact active centers.

Several methods have been suggested over the years to increase photocatalytic H_2 production, including copolymerization [20,21], cross-linker modification [22,23], donor–acceptor structure construction [24,25], functionalization [26,27], heterojunction fabrication [28–31], and surface modification [32,33]. There are primarily three types of photocatalytic mechanisms: improving the absorption of visible light, speeding up the efficient migration and separation of charges, and increasing the surface catalytic reaction. Additionally, electron–hole pair separation and transmission is the most important part of photocatalysis [34], although charge recombination is more likely to happen because CPs produce highly bound Frenkel excitons when exposed to sunlight [35,36]. By constructing heterostructures for CPs out of two different organic semiconductors, one feasible method for lowering the rate of electron–hole recombination can be implemented [37].

An example of this would be the incorporation of poly(3-hexylthiophene) (P3HT) with g-C_3N_4 in 2011 to create a heterojunction structure [38]. Subsequently, Shen et al. first integrated fluorene-based polymer (PcZF) with g-C_3N_4 to manufacture an organic heterostructure in order to increase exciton dissociation [39]. Using the two CPs, PTB7-Th and EH-IDTBR, McCulloch et al. recently described a heterojunction based on CPs that boosts PHE activity [40]. The heterojunction has a nano-interpenetrating network topology. The effectiveness of charge transfer across interfaces is dictated by the contact state; chemically bound heterostructures are more suited to improve this condition than non-covalent ones. In addition to the unique CTF-based molecular heterostructures produced by Li et al. and coworkers via a proof-of-concept trifluoromethanesulfonic acid (TfOH)-catalyzed trimerization [41], we present novel chemically bonded heterostructures based on a simple Schiff base reaction of substituted groups.

In this work, a novel method for the synthesis of chemically linked heterostructures comprising dibenzothiophene-S,S-dioxide, ethylene dioxythiophene, and benzenoid units was developed by use of the Schiff base reaction involving the substituent of the aldehyde functional group (CHO) and the substituent of amine (NH_2) (Scheme 1). The Schiff base reaction served as the foundation for this approach. The D-A structure, which consists of chemically bonded heterostructures with electron-donating moieties and electron-accepting groups, can speed up the separation and transfer of excitons, according to a thorough investigation of the correlations between structure, property, and performance. As a simple and popular way to increase the PHE of CP-based photocatalysts, the TPA-Ph@PPD-BSO_2 demonstrates an optimal HER of up to 16.5 mmol g^{-1} h^{-1} when exposed to visible light ($\lambda > 420$ nm).



Scheme 1. The procedures for the construction of heterostructures consisting of TPA-EDOT@PPD-BSO_2, TPA-BSO2@PPD-BSO_2, and TPA-Ph@PPD-BSO_2. The following compounds were investigated:

(i) $Pd(PPh_3)_4$, K_2CO_3, and DMF at 120 °C in an Ar atm; (ii) $Pd_2(dba)_3$, P(o-MeOPh)$_3$, Cs_2CO_3, PivOH, and toluene at 110 °C in an Ar atm; (iii) n-Butyl alcohol at 90 °C in an Ar atm.

2. Results and Discussion

2.1. Synthesis of Catalytic Compounds and Their Structural Analysis

The PPD-BSO_2 polymers with unreacted side-chain amino groups were originally produced by polymerizing 2,5-Dibromobenzene-1,4-diamine (PPD) and 3,7-bis(4,4,5,5-tetramethyl-1,3,2-dioxabor-olan-2-yl) dibenzothiophene-S,S-dioxide dibenzo[b,d]thiophene-S,S-dioxide (bso2) (Scheme 1). Afterwards, TPA-EDOT, TPA-BSO_2, and TPA-Ph were formed with unreacted side-chain aldehyde groups, respectively, by coupling 2,5-dibromo-1,4-diformylbenzene (TPA) with 3,4-Ethylenedioxythiophene (EDOT), 3,7-bis(4,4,5,5-tetramethyl-1,3,2-dioxabor-olan-2-yl)dibenzothiophene-S,S-dioxide diben-zo[b,d]thiophene-S,S-dioxide ($BTSO_2$), and 1,4-phenylenebisboronic acid (Ph), respectively. Finally, TPA-EDOT@PPD-BSO_2, TPA-BSO_2@PPD-BSO_2, and TPA-Ph@PPD-BSO_2 were constructed via the Schiff base reaction involving the -CHO from TPA-X and the -NH_2 from PPD-BSO_2. In addition, we synthesized several mechanical mixture samples, designated PPD-BSO_2+TPA-X.

As shown in Figure S1, the as-prepared COPs' FT-IR spectra exhibit bimodal characteristic peaks at 3300~3500 cm^{-1}, which are associated with the stretching vibrations of N-H. The peaks at ~1686 cm^{-1} correspond to the stretching vibrations of C=O. The characteristic signals of the sulfone group (O=S=O) from the BSO_2 unit are located at 1300 and 1155 cm^{-1}. Figure 1a displays the Fourier transform infrared (FT-IR) spectra of chemically linked heterostructures, specifically TPA-EDOT@PPD-BSO_2, TPA-BSO_2@PPD-BSO_2, and TPA-Ph@PPD-BSO_2, respectively. At approximately 1520 cm^{-1}, a new peak can be attributed to the presence of C=N bonds. The weakening of C=O and N-H stretching after chemically bonded heterostructures were formed suggests that PPD-BSO_2 and TPA-X (X = TPA-EDOT, TPA-BSO_2, and TPA-Ph) were successfully integrated. Subsequently, we also conducted comparative Fourier transform infrared (FT-IR) spectroscopy analysis of the covalent heterojunction PPD-BSO_2@TPA-Ph and the corresponding mechanical mixture PPD-BSO_2+TPA-Ph (Figure S1d). In PPD-BSO_2+TPA-Ph, the peak at ~1686 cm^{-1} is pronounced and weakens significantly in the PPD-BSO_2@TPA-Ph. This also indirectly confirms the successful occurrence of the Schiffer base condensation reaction at the interface. Figure 1b shows that representative samples were selected from the copolymers PPD-BSO_2, TPA-Ph, and TPA-Ph@PPD-BSO_2, and that the copolymer structures were verified using the solid-state ^{13}C NMR spectra. Approximately 136 ppm of the PPD-BSO_2 signal is attributed to the carbon atoms that are next to the N atoms, about 193 ppm to the carbon atoms that are next to the O atoms, and about 141 ppm to the carbon atoms that are bonding with the sulfur atoms in the BSO_2 chemical compound. It should be noted that the TPA-Ph@PPD-BSO_2 is composed of TPA and PPD components. A mechanical mixture of TPA-Ph and PPD-BSO_2 served as a control in the experiment, demonstrating the effectiveness of this synthetic method; however, chemically bound heterostructures TPA-Ph@PPD-BSO_2 displayed spectra resembling the mixture. In addition, it is clear that chemically bonded heterostructures were generated by PPD-BSO_2 and TPA-Ph, as evidenced by these observations (Figure S2).

Using scanning electron microscopy (SEM) and transmission electron microscopy (TEM), respectively, the morphologies of the TPA-EDOT@PPD-BSO_2, TPA-BSO_2@PPD-BSO_2, and TPA-Ph@PPD-BSO_2 hybrids were investigated at the micro- and nano-scales (Figure 2). The purpose of this was to discover how the amino groups interacted with the aldehyde groups to affect the morphology. The three components show different morphologies in the scanning electron microscopy pictures (Figure S3). PPD-BSO_2 has a nano-lamellar lamellar morphology, TPA-Ph exhibits an aggregated nano-particle spherical morphology, and TPA-Ph@PPD-BSO_2 has a nano-lamellar lamellar morphology with a

porous structure. Similar to the scanning electron microscopy (SEM) image, the transmission electron microscopy (TEM) picture of TPA-Ph@PPD-BSO_2 shows that the nanoparticulate of TPA-Ph covers the nanosheets of PPD-BSO_2. This provides more evidence that the two semiconductors are well-connected, supporting the underlying mechanism of the charge transfer. Chemically linked heterostructures have a nano-lamellar lamellar morphology with a porous structure, as seen in scanning electron microscopy (SEM) images, and a finer nanoribbon structure, as shown in the transmission electron microscopy (TEM) picture of TPA-Ph@PPD-BSO_2. Since the corresponding contact area would be larger in TPA-Ph@PPD-BSO_2, the finer nanoribbon structure would unquestionably aid the improved photocatalytic reactions.

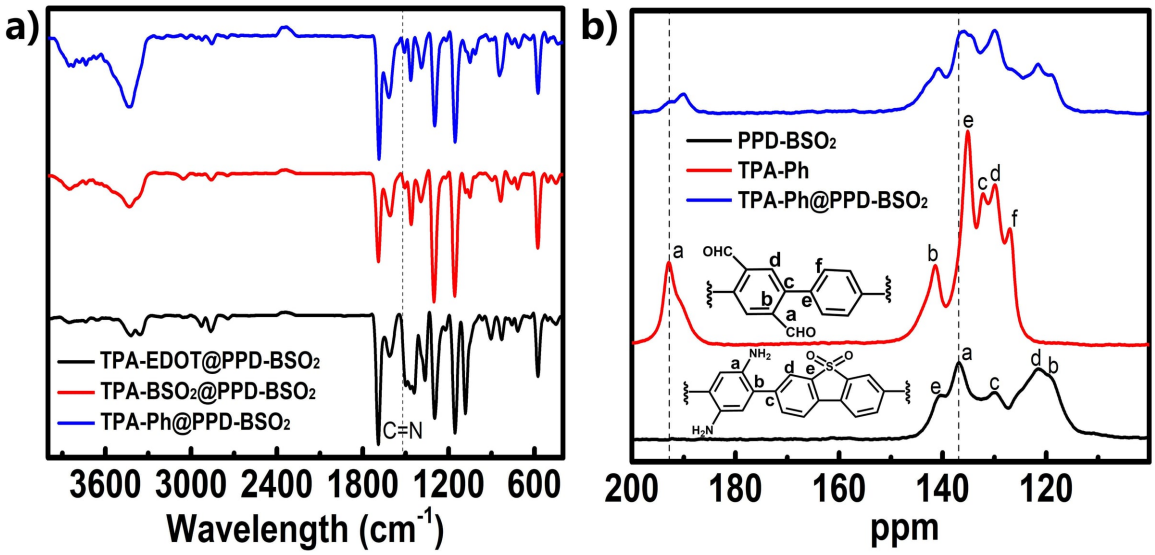


Figure 1. (**a**) FT-IR spectra of TPA-EDOT@PPD-BSO_2, TPA-BSO_2@PPD-BSO_2 and TPA-Ph@PPD-BSO_2; (**b**) solid-state ^{13}C NMR spectra of PPD-BSO_2, TPA-Ph, and TPA-Ph@ PPD-BSO_2.

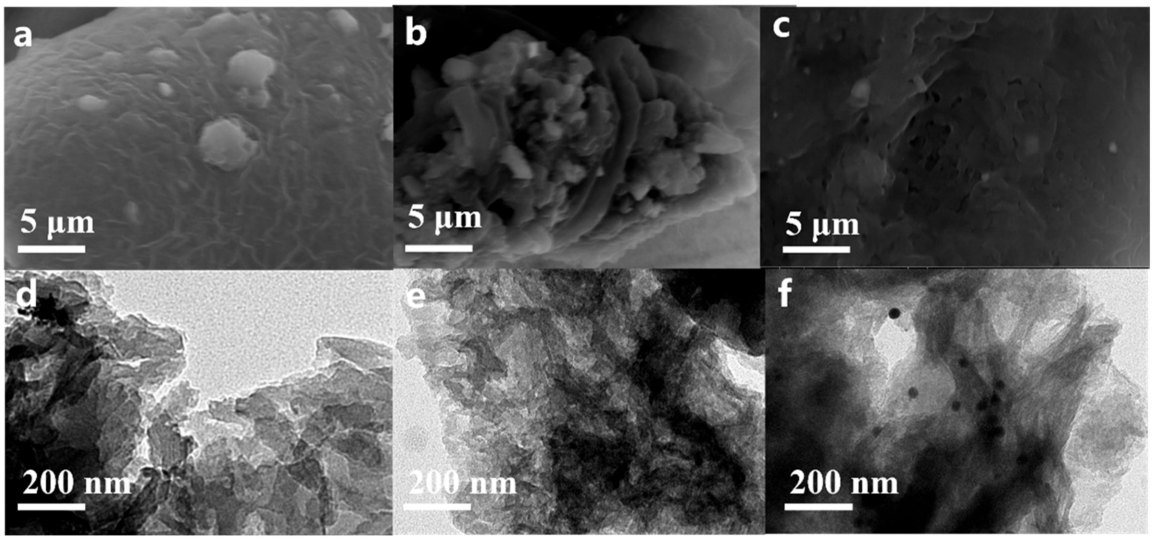


Figure 2. (**a**–**c**) SEM and (**d**–**f**) TEM of T PPD-BSO_2@TPA-EDOT, PPD-BSO_2@TPA-BSO_2 and PPD-BSO_2@TPA-Ph.

2.2. Optical and Electrochemical Properties

The conjugated organic polymers were studied for their photophysical properties using a variety of techniques, including transient photocurrent response (TPR), electro-

chemical impedance spectra (ESI) Nyquist plots, cyclic voltammetry (CV), steady-state photoluminescence (PL) spectra, ultraviolet–visible (UV-vis) diffuse reflectance spectra, and solid-state polymer powder. Figure 3a demonstrates that all of the polymers that are chemically attached to heterostructures have a clear potential to absorb ultraviolet and visible light (Figure 3a). It is evident that the chemically connected heterostructures largely absorbed the optical properties of the weaker one, leading to a modest bandgap, as the light absorption range of TPA-EDOT@PPD-BSO_2, TPA-BSO_2@PPD-BSO_2, and TPA-Ph@PPD-BSO_2 is in the middle of the two precursor polymers. According to Figure S4, the chemically bonded heterostructures of TPA-EDOT@PPD-BSO_2 have a red-shifted absorption compared to PPD-BSO_2, whereas TPA-BSO2@PPD-BSO_2 and TPA-Ph@PPD-BSO_2 have a blue-shifted absorption compared to PPD-BSO_2 (Figure S4). This is likely because TPA-EDOT has a stronger light absorption capacity due to the strong electron donor unit of EDOT.

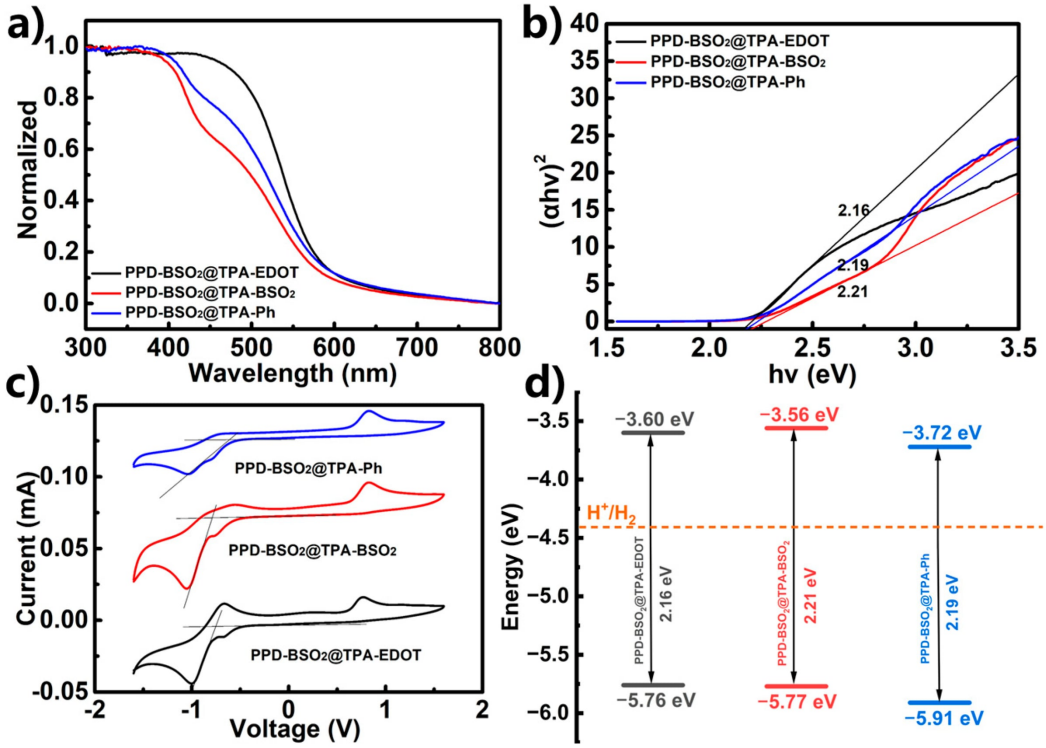


Figure 3. (**a**) UV-vis DRS; (**b**) Tauc plots; (**c**) CV; and (**d**) energy-level alignments of PPD-BSO_2@TPA-EDOT, PPD-BSO_2@TPA-BSO_2 and PPD-BSO_2@TPA-Ph.

The optical bandgaps (Eg) of the chemically linked heterostructures TPA-EDOT@PPD-BSO_2, TPA-BSO2@PPD-BSO_2, and TPA-Ph@PPD-BSO_2 were determined to be 2.16, 2.21, and 2.19 eV, respectively, according to the curves of $(\alpha h\nu)^2$ vs. hν plotted in Figure 3b. To investigate the electronic structure properties of three heterojunction polymers and four single polymers, cyclicvoltammetry (CV) was used to systematically characterize the front molecular orbital (FMO) energy-level distributions of the four polymers (Figures S5 and 3c). By using cyclic voltammetry (CV) and optical bandgaps (E_g), based on the equation $E_{LUMO} = E_{HOMO} - E_g$, the energy-level locations of the LUMO and HOMO states of the chemically coupled heterostructures were examined. The LUMO levels of PA-EDOT@PPD-BSO_2, TPA-BSO_2@PPD-BSO_2, and TPA-Ph@PPD-BSO_2 were −3.60, −3.56, and −3.72 eV, respectively. When looking at the chemically linked heterostructures with their predicted bandgaps, the HOMO levels of PA-EDOT@PPD-BSO_2, TPA-BSO_2@PPD-BSO_2, and TPA-Ph@PPD-BSO_2 were −5.76, −5.77, and −5.91 eV, respectively. The LUMO levels in each of the samples are appropriate, and there is a possible thermodynamic force that can drive the process that

produces hydrogen. In addition, the energy-level diagrams for the four single-component polymers are shown in the Figure S5. The LUMO levels of TPA-EDOT, TPA-BSO_2, TPA-Ph and PPD-SBO_2 were −3.60, −3.58, −3.73, and −3.63 eV, respectively. All four polymers meet the thermodynamic requirements for hydrogen production; however, in the case of the TPA-Ph polymer, factors such as kinetics and rapid carrier recombination may prevent it from meeting the conditions for hydrogen production.

Considering that photoluminescence is a photon-to-photon process, it is a straightforward and practical indicator that may be utilized to evaluate the recombination of photo induced electron–hole (e^--h+) pairs. Steady-state PL spectroscopy is widely used to evaluate radiative recombination of photogenerated charge carriers [42–48]. Figure 4a shows that TPA-Ph@PPD-BSO_2 has substantially lower photoluminescence (PL) intensity than TPA-EDOT@PPD-BSO_2 and TPA-BSO_2@PPD-BSO_2, indicating a distinct separation of photo generated electron–hole pairs. This is particularly problematic for photocatalysis, as stronger PL typically leads to more radiative recombination of e^--h+ couples. Using transient photocurrent responses (I-t) and electrochemical impedance spectra (EIS), the three-electrode cell setup was used to confirm the excellent catalytic performance and evaluate the electron transfer behavior of PA-EDOT@PPD-BSO_2, TPA-BSO2@PPD-BSO_2, and TPA-Ph@PPD-BSO_2. In comparison to TPA-EDOT@PPD-BSO_2 and TPA-BSO_2@PPD-BSO_2, the photocurrent density of TPA-Ph@PPD-BSO_2 indicated a substantially better photocurrent response, as evidenced by the I-t curves in Figure 4b. According to Figure 4c, electrochemical impedance spectroscopy (EIS) showed that compared to TPA-EDOT@PPD-BSO_2 and TPA-BSO_2@PPD-BSO_2, TPA-Ph@PPD-BSO_2 had a lower interfacial charge transfer resistance.

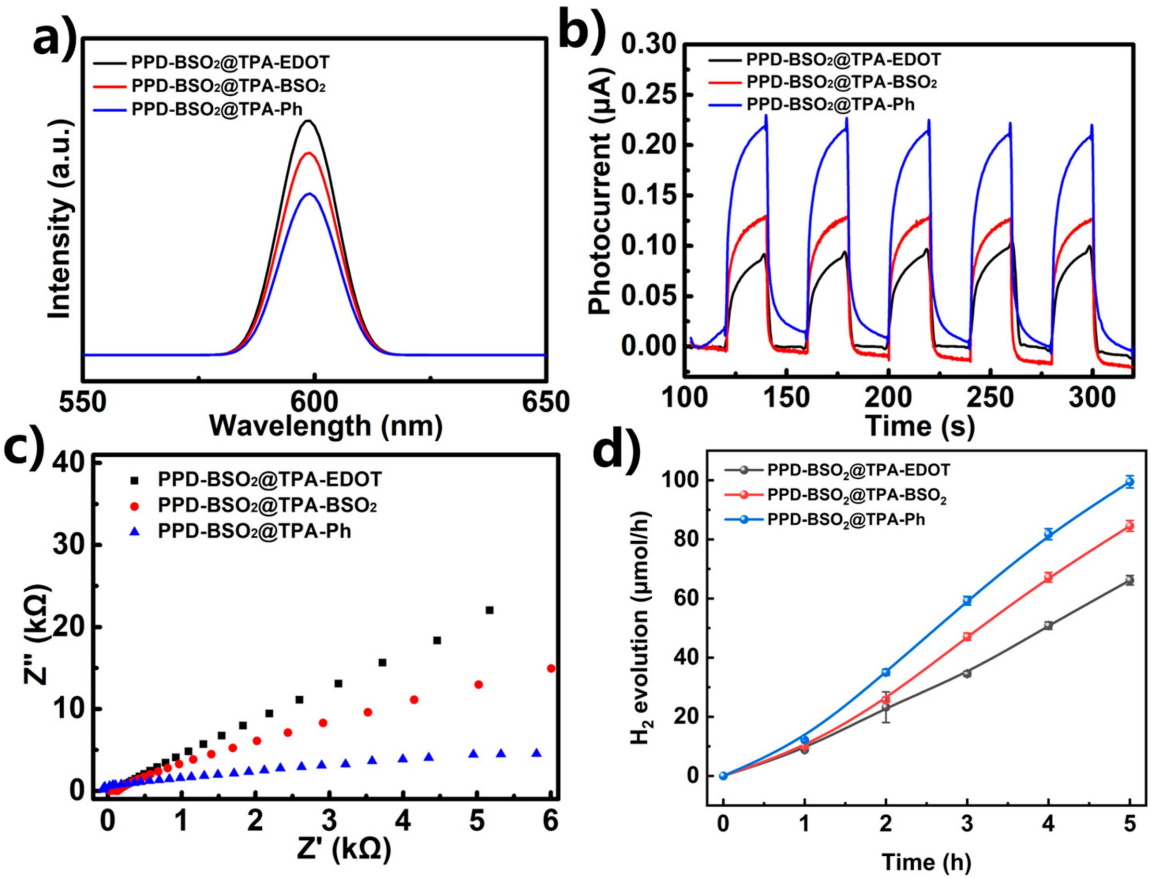


Figure 4. (**a**) PL spectra excited at 400 nm; (**b**) TPR; (**c**) EIS; and (**d**) HERs of TPA-EDOT @PPD-BSO_2, TPA-BSO_2@PPD-BSO_2 and TPA-Ph@PPD-BSO_2 in AA/H_2O.

It was demonstrated by all of the aforementioned findings that the chemically bound heterostructures of TPA-Ph@PPD-BSO_2 exhibited effective charge transfer and separation of ions. In a photocatalytic hydrogen production test, which did not include a Pt co-catalyst, the photocatalytic performance of the polymers was examined by measuring the amount of hydrogen produced using visible light irradiation with ascorbic acid (AA) as a sacrificial agent. The dosage of each polymer photocatalyst was 6 mg. According to Figure 4d, the hydrogen evolution rates (HER) of TPA-EDOT@PPD-BSO_2, TPA-BSO_2@ PPD-BSO_2, and TPA-Ph@PPD-BSO_2 are reported to be 66, 84.6, and 99 μmol h^{-1}, respectively. These values correspond to the normalized HERs of 11.0, 14.1, and 16.5 mmol h^{-1} g^{-1}, respectively. As shown in Figure S6, the single-component hydrogen evolution rates (HERs) of PPD-BSO_2, TPA-BSO_2, TPA-EDOT, TPA-Ph are reported to be 10.1, 6.2, 5.0 mmol h^{-1} g^{-1}, respectively. To demonstrate that covalent linkage, rather than simple physical contact, drives improved charge separation and HER, we evaluated three types of mechanically mixed photocatalysts under identical conditions. As illustrated in Figure S7, the mechanical PPD-BSO_2+TPA-Ph mixture exhibited a hydrogen evolution rate of only 10.8 mmol g^{-1} h^{-1}, which was comparable only to that of PPD-BSO_2 and markedly lower than that of the covalently bonded TPA-Ph@PPD-BSO2 (16.5 mmol g^{-1} h^{-1}). The mechanical PPD-BSO_2+TPA-EDOT and PPD-BSO_2+TPA-BSO_2 mixtures both exhibited hydrogen evolution rates lower than those of the covalently bonded mixtures. This direct comparison validates that the Schiff base covalent bonds serve as molecular electronic conduits, driving improved charge separation and thereby leading to more efficient hydrogen evolution.

2.3. Photocatalytic Hydrogen Production Performance

Photocatalytic performance is greatly impacted by the organic polymer photocatalysts' light absorption capacity; this finding is in good agreement with the UV-vis absorption spectra of TPA-Ph@PPD-BSO_2. Figure 5a shows that the maximum apparent quantum yield (AQY) at 500 nm for TPA Ph@PPD-BSO_2 fluctuates with the polymer's light absorption capacity, reaching 10.4% at that wavelength. As can be seen in Figure 5b, cycling measurements of HER over TPA-Ph@PPD-BSO_2 were carried out across four runs lasting twenty hours, with error bars ($n = 3$). The catalyst retained 85.1% of its initial rate in the fourth cycle. The slight decay is mainly attributable to partial consumption of the ascorbic acid sacrificial donor and minor mechanical loss during filtration/purging. The FT-IR UV-Vis and SEM analyses confirmed PPD-BSO_2@TPA-Ph retained its structural integrity and chemical structure stability after prolonged photocatalytic measurements (Figure S8).

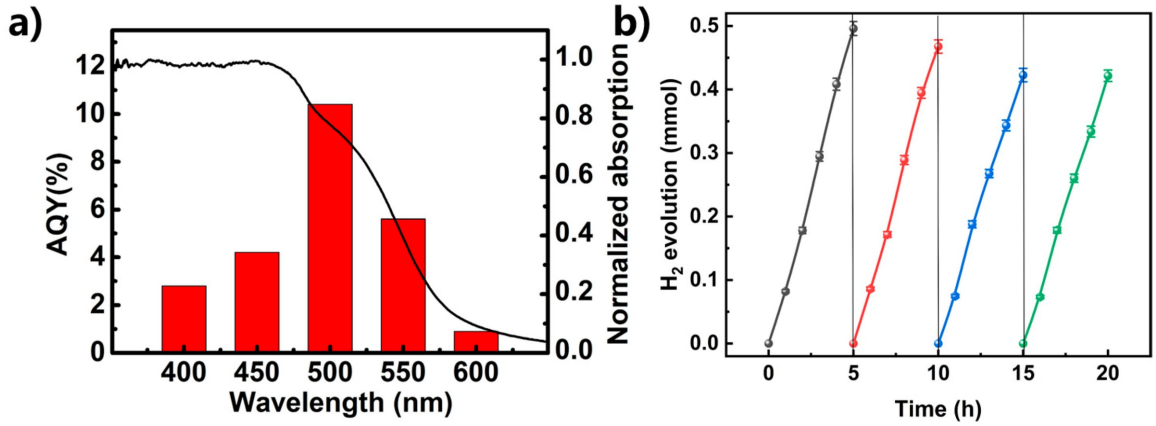


Figure 5. (**a**) AQYs; (**b**) recyclability of TPA-Ph@PPD-BSO_2 in AA/H_2O.

The difference in activity among the various composite polymers cannot be explained solely by the extent of visible light harvesting. Instead, charge-carrier separation dynamics

and interfacial energetics dominate. Figure 6 shows that chemically bonded heterostructures have substantially reduced PL intensities, as a result of adding EIS, TPR, and PL to the charge transfer property characterization of bonded heterostructures and precursor polymers. However, when TPA-EDOT, TPA-BSO_2, and TPA-Ph are integrated with PPD-BSO_2, the PL of these three compounds is effectively quenched. This suggests that the photogenerated charges of TPA-X, where X is the sum of TPA-EDOT, TPA-BSO_2, and TPA-Ph, are primarily transferred to PPD-BSO_2 via the Schiff base reaction involving the -CHO of TPA-X and the -NH_2 of PPD-BSO_2. To elucidate the charge separation and transfer dynamics, steady-state photoluminescence (PL) and electrochemical impedance spectroscopy (EIS) measurements were performed on the mechanical PPD-BSO_2+TPA-Ph mixture and heterojunction polymer PPD-BSO_2@TPA-Ph. As shown in Figure S9a, the mechanical PPD-BSO_2+TPA-Ph mixture displays a prominent emission peak centered at around 450 nm, which stems from the rapid radiative recombination of photogenerated electron–hole pairs. In sharp contrast, the PL intensity of the covalently linked heterojunction PPD-BSO_2@TPA-Ph is dramatically quenched, demonstrating substantially suppressed charge recombination and efficient charge dissociation across the interface. Furthermore, the EIS Nyquist plots (Figure S9b) reveal that PPD-BSO_2@TPA-Ph possesses a significantly smaller semicircular radius compared to the mechanical PPD-BSO_2+TPA-Ph mixture, indicating a drastically reduced charge transfer resistance. These combined results verify that the in situ-constructed covalent linkages effectively accelerate interfacial electron transfer and promote spatial separation of photogenerated carriers, fundamentally underpinning the superior photocatalytic performance.

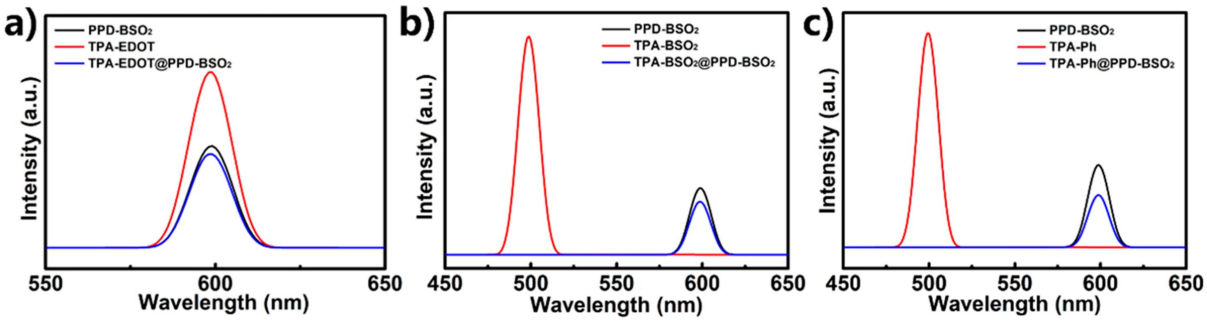


Figure 6. (**a**) PL spectra excited at 400 nm of PPD-BSO_2, TPA-EDOT, and TPA-EDOT@PPD-BSO_2; (**b**) PPD-BSO_2, TPA-BSO_2, and TPA-BSO_2@PPD-BSO_2; and (**c**) PPD-BSO_2, TPA-Ph, and TPA-Ph@ PPD-BSO_2.

Additional evidence for the chemically bound heterostructures' photocatalytic HER regularity came from studies of electrochemical impedance spectra and photocurrents. A comparatively strong photocurrent response was observed for all of the bonded heterostructures in comparison to the precursor polymers, as indicated by the I-t curves displayed in Figures S10a,b and 7a. The precursor polymers' interfacial charge transfer kinetics were studied using EIS measurement, and the bonded heterostructures outperformed them in terms of photocurrent intensity, indicating that they could generate more light-induced charges. Compared to the precursor polymers, the bonded heterostructures showed a smaller diameter in the Nyquist plot (Figures S10c,d and 7b), indicating a decreased interfacial charge transfer resistance. It was demonstrated by all of the aforementioned findings that the bonded heterostructures had the potential to greatly improve the electron–hole pair separation and transfer, which ultimately resulted in an increased effective energy ratio (Figure 7c).

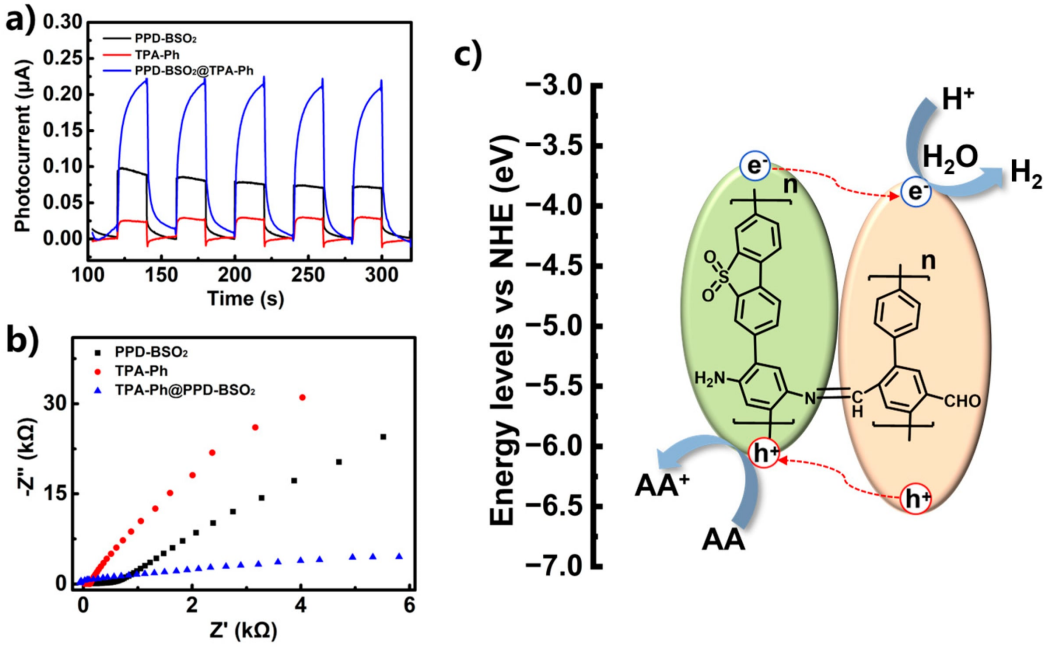


Figure 7. (**a**) TPR; (**b**) EIS; and (**c**) illustration of the facilitated charge-carrier separation across the chemically bonded heterostructures of PPD-BSO_2, TPA-Ph, and TPA-Ph@PPD-BSO_2.

3. Experimental

3.1. Materials and Methods

EDOT (98%), Cs_2CO_3 (99.9%), P(o-MeOPh)$_3$ (98%), Pd_2 (dba)$_3$ (98%), Pd$(PPh_3)_4$ (98%), PivOH (99%), K_2CO_3 (99%), AA (98%) and DMF were purchased from Energy Chemical Ltd. (Shanghai, China). $BTSO_2$ (98%) was purchased from TCI (Tokyo, Japan). MeOH and CH_2Cl_2 were purchased from XiLong Scientific (Shanghai, China). The solvents used were all analytic reagents (ARs) with 99% purity.

Typical procedure for the synthesis of CPs via DArP: After charging a Schlenk tube with the monomers P(o-MeOPh)$_3$, Cs_2CO_3, pivalic acid, and Pd_2(dba)$_3$, the mixed solid that was contained within the tube was purged via a series of vacuum- and argon-filling cycles. After adding anhydrous toluene to the tube using a syringe, the reaction mixture was subjected to three cycles of freezing–vacuum–thawing to eliminate dissolved gases. Subsequently, the mixture was vigorously agitated at 110 °C for 48 h while being maintained under an argon atmosphere. Following the mixture's cooling to room temperature, it was poured into CH_2Cl_2, and the precipitate was recovered using filtering. The precipitate was then washed with CH_2Cl_2, MeOH, and distilled water. For an additional 12 h at 80 °C in a vacuum furnace, the polymers were dried to obtain the final particle products, which were purified further by soaking in MeOH and CH_2Cl_2, respectively.

Typical procedure for the synthesis of CPs via Suzuki coupling: The monomers Pd$(PPh_3)_4$ and K_2CO_3 were charged into a Schlenk tube, and the mixed solid that was contained within the tube was purged by a series of vacuum- and argon-filling repetitions. After that, anhydrous toluene and a small amount of DMF were injected into the tube through a syringe, respectively. After three cycles of freezing, vacuuming, and thawing to extract any gases that may have dissolved in the reaction mixture, it was subjected to vigorous stirring at 120 °C for 48 h in an argon environment. After the mixture had been allowed to cool to room temperature, it was poured into CH_2Cl_2, and the precipitate was subsequently recovered by filtration and rinsed with CH_2Cl_2, MeOH, distilled water, and MeOH prior to being returned to the mixture. After the polymers were further purified by

soaking them in CH_2Cl_2, MeOH, distilled water, and MeOH, respectively, they were dried in a vacuum oven at 80 °C for 12 h to achieve the final powder products.

Typical procedure for the synthesis of Heterojunction Polymers via Schiff base reaction: Polymers bearing amino substituents TPA-X and polymers bearing aldehyde substituents PPD-BSO_2 were added in a specific ratio to a Schlenk tube. The mixture underwent three cycles of vacuum and argon purging via a double-row tube. Under an argon atmosphere, n-butanol was introduced into the reaction tube as the reaction solvent, followed by three additional cycles of freezing, vacuum, and argon purging. The mixture was stirred uniformly for 24 h in a 90 °C oil bath. After the reaction, the mixture was cooled to room temperature; the crude product was washed sequentially with dichloromethane and methanol to remove low-molecular-weight byproducts, and then vacuum-dried at 80 °C for 12 h.

Synthesis of TPA-EDOT via DArP: TPA (0.685 mmol, 200.0 mg), EDOT (1 equiv., 0.685 mmol, 97.4 mg), Cs_2CO_3 (2 equiv., 1.37 mmol, 446.4 mg), PivOH (30 mol%, 30.0 mg), $Pd_2(dba)_3$ (1.5 mol%, 12.5 mg), P(o-MeOPh)$_3$ (3 mol%,9.6 mg), and 10 mL anhydrous toluene were used to synthesize TPA–EDOT via DArP. The product was obtained as an orange powder (150 mg, 80.5%).

Synthesis of PPD-BSO_2 via Suzuki coupling: PPD (1.28 mmol, 340.8 mg), BSO_2-Bpin (1 equiv., 1.28 mmol, 600 mg), K_2CO_3 (3 equiv., 3.84 mmol, 530.5 mg), Pd$(PPh_3)_4$ (5 mol%, 74 mg), and 14 mL DMF were used to synthesize PPD-BSO_2 via Suzuki coupling. The product was obtained as a red-orange powder (400 mg, 88.7%).

Synthesis of TPA-BSO_2 via Suzuki coupling: TPA (0.685 mmol, 200 mg), BSO2-Bpin (1 equiv., 0.685 mmol, 320.7 mg), K_2CO_3 (3 equiv., 2.05 mmol, 283.6 mg), Pd$(PPh_3)_4$ (5 mol%, 39.6 mg), and 10 mL DMF were used to synthesize TPA-BSO_2 via Suzuki coupling. The product was obtained as a luminous yellow powder (214 mg, 79.8%).

Synthesis of TPA-Ph via Suzuki coupling: TPA (0.685 mmol, 200 mg), Ph (1 equiv., 0.685 mmol, 113.5 mg), K_2CO_3 (3 equiv., 2.05 mmol, 283.6 mg), Pd$(PPh_3)_4$ (5 mol%, 39.6 mg), and 10 mL DMF were used to synthesize TPA-Ph via Suzuki coupling. The product was obtained as a luteotestaceous powder (105 mg, 84.2%).

Synthesis of TPA-EDOT@PPD-BSO_2 via Schiff base reaction: PPD-BSO_2 (1 equiv., 0.312 mmol, 100 mg), TPA-EDOT (1 equiv., 0.312 mmol, 85.0 mg), and 4 mL n-Butyl alcohol were used to synthesize TPA-EDOT@PPD-BSO_2 via a Schiff base reaction. The product was obtained as a red-orange powder (106.3 mg, 60%).

Synthesis of TPA-BSO_2 @PPD-BSO_2 via Schiff base reaction: PPD-BSO_2 (1 equiv., 0.312 mmol, 100 mg), TPA-BSO_2 (1 equiv., 0.312 mmol, 108.1 mg), and 4 mL n-Butyl alcohol were used to synthesize TPA-BSO_2@PPD-BSO_2 via a Schiff base reaction. The product was obtained as a yellow powder (105.5 mg, 50%).

Synthesis of TPA-Ph@PPD-BSO_2 via Schiff base reaction: PPD-BSO_2 (1 equiv., 0.312 mmol, 100 mg), TPA-Ph (1 equiv., 0.312 mmol, 65.0 mg), and 4 mL n-Butyl alcohol were used to synthesize TPA-Ph@PPD-BSO_2 via a Schiff base reaction. The product was obtained as a saffron yellow powder (114.5 mg, 72%).

3.2. Photocatalytic Hydrogen Production Tests

Following the addition of 30 mL of water containing 5 g of AA, 6 mg of photocatalyst was ultrasonically dispersed in water in the PHP reaction vessel for a period of ten minutes. In order to maintain a vacuum, the mixture was degassed, and then it was irradiated with a 300 W Xe lamp (MC-PF300C, Beijing Merry Change Technology, Beijing, China). When the temperature of the reaction mixture was maintained at 25 °C, PHP performances were evaluated using an online analysis system (MC-SPB10, Beijing Merry Change Technology, Beijing, China). An online gas chromatograph (GC9790, FuLi, Wenzhou, China) equipped

with a thermal conductivity detector (TCD) and working with argon as the carrier was utilized in order to determine the quantity of hydrogen that was created. Filters of 400 nm, 450 nm, 500 nm, 550 nm and 600 nm were implanted at the light source, the photocatalytic reactor was continuously irradiated at each wavelength for two hours, and the apparent quantum yields at different wavelengths were measured and recorded. The light intensity of the light source was measured using a standard power meter (Model 843R, Newport, Perfect light, Beijing, China). The apparent quantum yield was calculated according to the following equation:

$$AQY = \frac{number\ of\ evolved\ H_2\ molecules}{number\ of\ incident\ photons} \times 100\% = \frac{2M \times N_A \times h \times c}{S \times P \times t \times \lambda} \times 100\%$$

where M is the amount of H_2 molecules (mol); N_A is the Avogadro constant (6.022 × 1023 mol^{-1}); h is the Planck constant (6.626 × 10^{-34} J·s); c is vacuum light velocity (2.997 × 108 m·s^{-1}); the irradiation area (S) is 25.5 cm^2 in our experiment; P is the intensity of the irradiating light (W·cm^{-2}); t is the photoreaction time (s); and λ is the wavelength of the monochromatic light (m).

4. Conclusions

In conclusion, we have demonstrated a post-synthetic Schiff base condensation strategy to construct covalently linked polymer–polymer heterojunctions using linear conjugated polymers containing complementary terminal aldehyde and amine functionalities. FT-IR spectra and solid-state ^{13}C NMR, alongside comparisons with a mechanical control mixture, confirm the successful synthesis of polymer heterojunctions. The charge-carrier-separation efficiency of the synthesized TPA-X@PPD-BSO_2 (TPA-EDOT, TPA-BSO_2, and TPA-Ph) materials was significantly enhanced because their bandgap alignment was scattered throughout the heterojunction. In the presence of visible light, TPA-Ph@PPD-BSO_2 demonstrated an optimum HER of up to 16.5 mmol g^{-1} h^{-1}, surpassing both its constituent precursors and the mechanical control mixture. Studies examining the relationship between structure, properties, and performance using UV-vis DRS, SEM, TEM, TPR, and EIS demonstrated that TPA-X@PPD-BSO_2 could enhance the photoinduced separation and transfer of charges in chemically bonded heterostructures, leading to remarkable photocatalytic performance. This is an effect that cannot be achieved through simple physical mixing. The contribution of this study is that it offers significant guidance for the design and adjustment of COPs.

Supplementary Materials: The following supporting information can be downloaded at https://www.mdpi.com/article/10.3390/molecules31234286/s1. Fourier transform infrared (FTIR) spectrograms of all polymers, solid-state ^{13}C NMR spectra of all polymers, SEM and TEM of all polymers, UV-vis DRS of all polymers, HERs of all polymers, and TPR and EIS of all polymers.

Author Contributions: Methodology and synthesis, Z.-T.B. and Y.-J.Z.; manuscript drafting, Y.-J.Z., Z.-T.B. and P.M.; photocatalytic hydrogen production test, Y.-J.Z.; data analysis, Z.-T.B.; conceptualization, S.-Y.L.; writing—review and editing, L.-Q.L. and S.-Y.L.; supervision, S.-Y.L.; project administration, K.-M.L., F.Y. and S.-Y.L.; funding acquisition, K.-M.L., L.-Q.L. and S.-Y.L. S.-Y.L. provided guidance during all stages. All authors have read and agreed to the published version of the manuscript.

Funding: This research was funded by the Jiangxi Provincial Natural Science Foundation (20252BAC250044) and the Guangdong Basic and Applied Basic Research Foundation (No. 2026A1515012021).

Institutional Review Board Statement: Not applicable.

Informed Consent Statement: Not applicable.

Data Availability Statement: Data are contained within the article and the Supplementary Materials.

Conflicts of Interest: The authors declare no conflicts of interest.

References

1. Turner, J.A. Sustainable Hydrogen Production. *Science* **2004**, *305*, 972–974. [CrossRef] [PubMed]
2. Chen, X.; Shen, S.; Guo, L.; Mao, S.-S. Semiconductor-based Photocatalytic Hydrogen Generation. *Chem. Rev.* **2010**, *110*, 6503–6570. [CrossRef] [PubMed]
3. Wang, Q.; Domen, K. Partiulate Photocatalystsfor Lght-Driven Water Spliting: Mechanisms, Challenges, and Design Stategies. *Chem. Rev.* **2020**, *120*, 919–985. [PubMed]
4. Chen, S.; Takata, T.; Domen, K. Particulate photocatalysts for overall water splitting. *Nat. Rev. Mater.* **2017**, *2*, 17050. [CrossRef]
5. Kudo, A.; Miseki, Y. Heterogeneous photocatalyst materials for water splitting. *Chem. Soc. Rev.* **2009**, *38*, 253–278. [CrossRef] [PubMed]
6. Wang, X.; Maeda, K.; Thomas, A.; Takanabe, K.; Xin, G.; Carlsson, J.M.; Domen, K.; Antonietti, M. A metal-free polymeric photocatalyst for hydrogen production from water under visible light. *Nat. Mater.* **2009**, *8*, 76–80. [CrossRef] [PubMed]
7. Wang, L.; Zhang, Y.; Chen, L.; Xu, H.; Xiong, Y. 2D Polymers as Emerging Materials for Photocatalytic Overall Water Splitting. *Adv. Mater.* **2018**, *30*, 1801955. [CrossRef] [PubMed]
8. Jayakuma, J.; Chou, H.-H. Recent Advances in Visible-Light-Driven Hydrogen Evolution from Water using Polymer Photocataysts. *ChemCaChem* **2020**, *12*, 689–704. [CrossRef]
9. Banerjee, T.; Podjaski, F.; Kroger, J.; Biswal, B.P.; Lotsch, B.V. Polymer photocatalysts for solar-to-chemical energy conversion. *Nat. Rev. Mater.* **2021**, *6*, 168–190. [CrossRef]
10. Wang, T.; Zhao, R.; Yang, Y.; Ren, H.; Lv, W.; Xu, H.; Liu, J. Enhanced Hydrogen-Rich Syngas Production Through In-Situ Heavy OilGasification Process Using Nanoscale Nickel Catalyst. *Molecules* **2025**, *30*, 809. [CrossRef] [PubMed]
11. Liu, Y.; Jia, Y.; Jia, H.; Gao, L. Recent Development on the Synthesis Strategies and Mechanisms of Co3O4-Based Electrocatalysts for Oxygen Evolution Reaction: A Review. *Molecules* **2025**, *30*, 3238. [CrossRef] [PubMed]
12. Shibata, T.; Kabumoto, A.; Shiragami, T.; Ishitani, O.; Pac, C.; Yanagida, S. Novel visible-light-driven photocatalyst. Poly(p-phenylene)-catalyzed photoreductions of water, carbonyl compounds, and olefins. *J. Phys. Chem.* **1990**, *94*, 2068–2076. [CrossRef]
13. Zhang, G.; Lan, Z.-A.; Wang, X. Conjugated Polymers: Catalysts for Photocatalytic Hydrogen Evolution. *Angew. Chem. Int. Ed.* **2016**, *55*, 15712–15727. [CrossRef] [PubMed]
14. Sprick, R.S.; Bonillo, B.; Clowes, R.; Guiglion, P.; Brownbill, N.J.; Slater, B.J.; Blanc, F.; Zwijnenburg, M.A.; Adams, D.J.; Cooper, A.I. Visible-Light-Dirven Hydrogen Evolution Using Planarized Conjugated Polymer Photocatalysts. *Angew. Chem. Int. Ed.* **2016**, *55*, 1792–1796. [CrossRef] [PubMed]
15. Hu, Z.; Wang, Z.; Zhang, X.; Tang, H.; Liu, X.; Huang, F.; Cao, Y. Conjugated Polymers with Oligoethylene Glycol SideChains for Improved Photocatalytic Hydrogen Evolution. *iScience* **2019**, *13*, 33–42. [CrossRef] [PubMed]
16. Lan, Z.-A.; Zhang, G.; Chen, X.; Zhang, K.A.I.; Wang, X. Reducing the exciton binding energy of donor-acceptor-based conjugated polymers to promote charge inducedreactions. *Angew. Chem. Int. Ed.* **2019**, *58*, 10236–10240. [CrossRef] [PubMed]
17. Dai, C.; Pan, Y.; Liu, B. Conjugated Polymer Nanomaterials for Solar Water Splitting. *Adv. Energy Mater.* **2020**, *10*, 2002474. [CrossRef]
18. Tan, Z.-R.; Xing, Y.-Q.; Cheng, J.-Z.; Zhang, G.; Shen, Z.-Q.; Zhang, Y.-J.; Liao, G.; Chen, L.; Liu, S.-Y. EDOT-based conjugated polymers accessed via C-H directarylation for efficient photocatalytic hydrogen production. *Chem. Sci.* **2022**, *13*, 1725–1733. [CrossRef] [PubMed]
19. Xie, Z.-H.; Zhang, Y.-J.; Li, J.; Liu, S.-Y. D1-A-D2 Conjugated Porous Polymers Provide Additional ElectronTransfer Pathways for Efficient Photocatalytic Hydrogen Production. *Molecules* **2025**, *30*, 2190. [CrossRef] [PubMed]
20. Sprick, R.S.; Aitchison, C.M.; Berardo, E.; Turcani, L.; Wilbraham, L.; Alston, B.M.; Jelfs, K.E.; Zwijnenburg, M.A.; Cooper, A.I. Maximising the hydrogen evolution activity in organic photocatalysts by co-polymerisation. *J. Mater. Chem. A* **2018**, *6*, 11994–12003. [CrossRef]
21. Sprick, R.S.; Jiang, J.-X.; Bonillo, B.; Ren, S.; Ratvijitvech, T.; Guiglion, P.; Zwijnenburg, M.A.; Adams, D.J.; Cooper, A.I. Tunable Organic Photocatalysts for Visible-Light-Driven Hydrogen Evolution. *J. Am. Chem. Soc.* **2015**, *137*, 3265–3270. [CrossRef] [PubMed]
22. Wang, Z.J.; Ghasimi, S.; Landfester, K.; Zhang, K.A.I. Molecular Structural Design of Conjugated Microporous Poly(Benzooxadiazole) Networks for Enhanced Photocatalytic Activity with Visible Light. *Adv. Mater.* **2015**, *27*, 6265–6270. [CrossRef] [PubMed]
23. Elewa, A.M.; Elsayed, M.H.; EI-Mahdy, A.F.M.; Chang, C.-L.; Ting, L.-Y.; Chou, H.-H. Triptycene-based discontinuously-conjugated covalentorganic polymer photocatalysts for visible-light-drivenhydrogen evolution from water. *Appl. Catal. B* **2021**, *285*, 119802. [CrossRef]

24. Liu, Y.; Liao, Z.; Ma, X.; Xiang, Z. Ultrastable and Efficient Visible-Light-Driven Hydrogen Production Based on Donor-Acceptor Copolymerized Covalent Organic Polymer. *ACS Appl. Mater. Interfaces* **2018**, *10*, 30698–30705. [CrossRef] [PubMed]
25. Shen, Z.-Q.; Xing, Y.-Q.; Chen, Y.; Zhang, G.; Liu, S.-Y. Nanoporous and nonporous conjugated donor-acceptorpolymer semiconductors for photocatalytic hydrogenproduction. *Beilstein J. Nanotechnol.* **2021**, *12*, 607–623. [CrossRef] [PubMed]
26. Sprick, R.S.; Bai, Y.; Guilbert, A.A.Y.; Zbiri, M.; Aitchison, C.M.; Wilbraham, L.; Yan, Y.; Woods, D.J.; Zwijnenburg, M.A.; Cooper, A.I. Photocatalytic Hydrogen Evolution from Water Using Fluorene and Dibenzothiophene Sulfone-Conjugated Microporous and Linear Polymers. *Chem. Mater.* **2019**, *31*, 305–313. [CrossRef]
27. Cheng, Z.; Zheng, K.; Lin, G.; Fang, S.; Li, L.; Bi, J.; Shen, J.; Bi, J. Constructing a novel family of halogen-doped covalenttriazine-based frameworks as efficient metal-freephotocatalysts for hydrogen production. *Nanoscale Adv.* **2019**, *1*, 2674–2680. [CrossRef] [PubMed]
28. Xu, Q.; Zhang, L.; Cheng, B.; Fan, J.; Yu, J. S-Scheme Heterojunction Photocatalyst. *Chem* **2020**, *6*, 1543–1559. [CrossRef]
29. Xing, Y.-Q.; Liu, S.-Y. Recent Progress in π-Conjugated Polymer-Inorganic Heterostructures for Photocatalysis. *Chin. J. Struct. Chem.* **2022**, *41*, 2209056–2209068.
30. Liao, G.; Li, C.; Liu, S.-Y.; Fang, B.; Yang, H. Z-scheme systems: From fundamental principles tocharacterization, synthesis, and photocatalytic fuel-conversion applications. *Phys. Rep.* **2022**, *983*, 1–41. [CrossRef]
31. Cai, C.; Sun, Y.; Xiao, Y.; Zheng, W.; Wang, W. Interface Engineering of ZnO-Decorated ZnFe2O4 for Enhanced CO2 Reduction Performance. *Molecules* **2025**, *30*, 3980. [CrossRef] [PubMed]
32. Cheng, J.-Z.; Liu, L.-L.; Liao, G.; Shen, Z.-Q.; Tan, Z.-R.; Xing, Y.-Q.; Li, X.-X.; Yang, K.; Chen, L.; Liu, S.-Y. Achieving an unprecedented hydrogen evolution rate bysolvent-exfoliated CPP-based photocatalysts. *J. Mater. Chem. A* **2020**, *8*, 5890–5899. [CrossRef]
33. Wang, X.; Zhao, X.; Dong, W.; Zhang, X.; Xiang, Y.; Huang, Q.; Chen, H. Integrating amino groups within conjugated microporouspolymers by versatile thiol-yne coupling for light-drivenhydrogen evolution. *J. Mater. Chem. A* **2019**, *7*, 16277–16284. [CrossRef]
34. Zhang, P.; Wang, T.; Chang, X.; Gong, J. Effective Charge Carrier Utilizationin Photocatalytic Conversions. *Acc. Chem. Res.* **2016**, *49*, 911–921. [CrossRef] [PubMed]
35. Mikhnenko, O.V.; Blom, P.W.M.; Nguyen, T.-Q. Exciton diffusion in organic semiconductors. *Energy Environ. Sci.* **2015**, *8*, 1867–1888. [CrossRef]
36. Li, H.-W.; Guan, Z.; Cheng, Y.; Lui, T.; Yang, Q.; Lee, C.-S.; Chen, S.; Tsang, S.-W. On the Study of Exciton Binding Energy with Direct Charge Generation in Photovoltaic Polymers. *Adv. Electron. Mater.* **2016**, *2*, 1600200. [CrossRef]
37. Zhang, X.; Peng, B.; Zhang, S.; Peng, T. Biomass Nanomicelles Assist Conjugated Polymers/PtCocatalysts To Achieve High Photocatalytic HydrogenEvolution. *ACS Sustain. Chem. Eng.* **2015**, *3*, 1501–1509.
38. Yan, H.; Huang, Y. Polymer composites of carbon nitride and poly (3-hexylthiophene) to achieve enhanced hydrogenproduction from water under visible light. *Chem. Commun.* **2011**, *47*, 4168–4170. [CrossRef] [PubMed]
39. Chen, J.; Dong, C.-L.; Zhao, D.; Huang, Y.-C.; Wang, X.; Samad, L.; Dang, L.; Shearer, M.; Shen, S.; Guo, L. Molecular Design of Polymer Heterojunctions for Efficient Solar-Hydrogen Conversion. *Adv. Mater.* **2017**, *29*, 1606198. [CrossRef] [PubMed]
40. Kosco, J.; Bidwell, M.; Cha, H.; Martin, T.; Howells, C.T.; Sachs, M.; Anjum, D.H.; Gonzalez Lopez, S.; Zou, L.; Wadsworth, A.; et al. Enhanced photocatalytic hydrogen evolution from organic semiconductor heterojunction nanoparticles. *Nat. Mater.* **2020**, *19*, 559–565. [CrossRef] [PubMed]
41. Huang, W.; He, Q.; Hu, Y.-P.; Li, Y.-G. Molecular Heterostructures of Covalent TriazineFrameworks for Enhanced Photocatalytic HydrogenProduction. *Angew. Chem. Int. Ed.* **2019**, *58*, 8676–8680. [CrossRef] [PubMed]
42. Li, L.; Zhang, Z.; Ding, C.; Xu, J. Boosting charge separation and photocatalytic CO_2 reduction of $CsPbBr_3$ perovskite quantum dots by hybridizing with P_3HT. *Chem. Eng. J.* **2021**, *419*, 129543. [CrossRef]
43. Dai, Y.; Zhou, Y.; Bao, Z.; Yu, C.; Li, J.; Yang, F.; Xie, Z.; Liu, S.-Y. Dipole-directed J-aggregation of atomically precise donor–acceptor molecules enables built-in-electric-field-driven multifunctional photocatalysis. *Appl. Catal. B Environ. Energy* **2027**, *401*, 127368. [CrossRef]
44. Zhao, W.; Luo, L.; Cong, M.; Liu, X.; Zhang, Z.; Bahri, M.; Li, B.; Yang, J.; Yu, M.; Liu, L.; et al. Nanoscale covalent organic frameworks for enhanced photocatalytic hydrogen production. *Nat. Commun.* **2024**, *15*, 6482. [CrossRef] [PubMed]
45. Isac, L.; Cazan, C. Current Research on MoS2-Based Heterojunction Photocatalysts for Persistent Organic Pollutants Degradation. *Molecules* **2025**, *30*, 4727. [CrossRef] [PubMed]
46. Xie, Z.; Dai, Y.; Bao, Z.; Zhou, Y.; Li, J.; Deng, L.; Yang, F.; Yu, C.; Liu, S.-Y. pH-Switchable Recoverable Quasi-Homogeneous Hydrophilic Polymeric Photocatalysts for Efficient Hydrogen Production. *Adv. Funct. Mater.* **2026**, *36*, e75860. [CrossRef]

47. Cheng, R.; Wang, Y.; Lu, S. Synergistic Enhancement of Photocatalytic H2O2 Production over CarbonNitride Oxide/Biochar Composites. *Molecules* **2025**, *30*, 4323. [CrossRef] [PubMed]
48. Xie, Z.-H.; Ye, G.; Gong, H.; Murugan, P.; Lang, C.; Dai, Y.-F.; Yang, K.; Liu, S.-Y. Ultrahigh photocatalytic hydrogen evolution oflinear conjugated terpolymers enabled by an ultra-low ratio of the benzothiadiazole monomert. *Chem. Sci.* **2025**, *16*, 9998. [CrossRef] [PubMed]

Disclaimer/Publisher's Note: The statements, opinions and data contained in all publications are solely those of the individual author(s) and contributor(s) and not of MDPI and/or the editor(s). MDPI and/or the editor(s) disclaim responsibility for any injury to people or property resulting from any ideas, methods, instructions or products referred to in the content.